Effects of cosolvent partitioning on conformational transitions and chain flexibility of thermoresponsive microgels

Peng-wei Zhu[1,*] and Luguang Chen[2]
[1]*Department of Materials Science and Engineering, Monash University, Clayton, VIC 3800, Australia*
[2]*Department of Chemical Engineering, Monash University, Clayton, VIC 3800, Australia*

(Received 24 November 2018; published 11 February 2019)

The conformational collapse of polymers in mixtures of two individually good solvents is an intriguing yet puzzling phenomenon termed *cononsolvency*. In this paper, the concept of the preferential adsorption of the cosolvent is combined with mean-field approaches to elaborate the cononsolvency effect of dimethylformamide (DMF) on the thermoresponsive poly(*N*-isopropylacrylamide) (PNIPAM) microgels in aqueous solutions. We give a quantitative description concerning the effects of DMF preferential adsorption and partitioning on the reentrant transition of PNIPAM microgels below the lower critical solution temperature (LCST) of PNIPAM. While the DMF cononsolvency incurs the conformational collapse, the affinity of DMF molecules to PNIPAM chains becomes increasingly stronger, which reveals that the conformational collapse is decoupled from the solvent quality of DMF-water mixtures. Considering the chain elasticity, spatial constraints, and surface charge of microgels, we explore the cononsolvency effect on the persistence length quantifying the PNIPAM flexibility. Our analysis elucidates that, depending on chain length and temperature, the DMF cononsolvency-induced collapse of PNIPAM microgels leads to a remarkable increase in the persistent length below LCST, which is comparable to the experimental data regarding suspension mechanical properties of PNIPAM microgels in water above LCST.

DOI: 10.1103/PhysRevE.99.022501

I. INTRODUCTION

Polymer microgels are soft particles of crosslinked chains with colloidal dimensions which are dispersed in water [1]. Thermoresponsive microgels have attracted increasing attention because they underlie a wide variety of applications in biomedical, functional, and environmental materials [2–5]. Important applications of thermoresponsive microgels are attributed to their two distinctive features. The first is thermal stability compared with linear counterparts. Individual microgels are stable during the conformational collapse due to the electrostatic repulsion between microgels, whereas the coil-to-globule transition of linear polymers is disturbed by phase separation. Second, compared to macrogels, characteristic times required to undergo the conformational transitions are much shorter in microgels than those in macrogels. As an example, these features can be well epitomized by poly(*N*-isopropylacrylamide) (PNIPAM), which has a lower critical solution temperature (LCST) at $T_{\mathrm{LCST}} \approx 305$ K [6]. As such, stable PNIPAM microgels can be quickly switched between swollen and collapsed states near ambient temperature in pure water [1].

Mixed solvents are ubiquitous in diverse applications to control or to optimize designed properties of polymeric materials. In this context, an intriguing yet puzzling phenomenon termed *cononsolvency* emerges when a second solvent or cosolvent is added to PNIPAM aqueous solutions at $T < T_{\mathrm{LCST}}$ [7–15]. Cononsolvency is the conformational collapse of a polymer in mixtures of two individually good solvents. In this sense, in addition to external stimuli such as temperature and pH, cononsolvency is considered as a good example of smart materials responding to the variation of cosolvent or solvent concentration.

Experimental investigations concerned with cononsolvency have depicted some common scenarios. All the cosolvents are water-miscible organic compounds which are good solvents, or even better than water, for PNIPAM. Cosolvents that have been often used are referred to as *kosmotropes* but some of them are classified as *chaotropes* [13]. In view of phase diagrams, some systems display a LCST behavior over the entire concentration range of the cosolvent, x_c, whereas more show the LCST behavior at lower x_c and the upper critical solution temperature at higher x_c [10]. Cononsolvency exhibits a collapse-reswelling or reentrant transition with the collapse in the water-rich region. In contrast to a solvent-excluded process of conventional collapse at $T > T_{\mathrm{LCST}}$, cononsolvency leads to a cosolvent- or solvent-included collapsed state at $T < T_{\mathrm{LCST}}$. When temperature is higher than T_{LCST}, cononsolvency does not exist any longer [12,15] and the addition of cosolvents triggers the swelling transition of already collapsed PNIPAM. To highlight the distinctive features, the cononsolvency effects on polymer networks are schematically contrasted with the conventional collapse (Fig. 1).

Two mechanisms have been proposed to explain the cononsolvency phenomenon. The indirect contact mechanism explains cononsolvency as a consequence of changes in water networks [9,10] in terms of kosmotropic effect [16], i.e., ordered cosolvent-water complexes weaken the solvation of

*zhupengwei@gmail.com

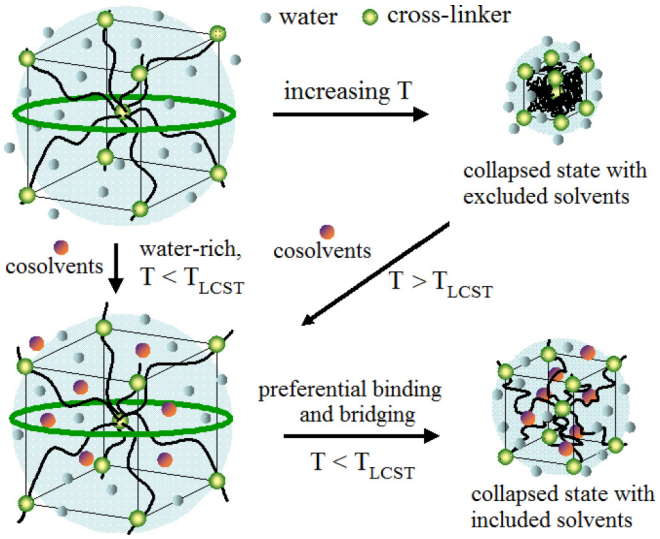

FIG. 1. Schematic of the cononsolvency effect on polymer networks and corresponding cosolvent- and solvent-included collapsed states. A microgel is composed of N_{ch}/p unit cells of p chains. Assume that the unit cell is a bcc of eight semiflexible chains ($p = 8$) [31].

hydrophobic moieties of PNIPAM, which drives the conformational collapse. The direct contact mechanism indicates that cosolvent molecules are directly involved in local interactions with polymer chains. In this context, the preferential adsorption crosslinking or bridging of cosolvent molecules to polymer chains give rise to the effective monomer-monomer attraction, which incurs the conformational collapse [11,14,15].

Accompanied by the experimental findings, the elaborate development of theoretical and computational investigations has provided deep insights to help elucidate the cononsolvency phenomenon. They include cooperative hydrogen-bonding effects [17], preferential adsorption and binding [18,19], Flory-Huggins type mean-field theory [8], the solvent-cosolvent interaction parameter [20], and Wyman-Tanford preferential binding [21], to name a few. For constrained polymer systems, which are of particular relevance to this paper, the direct contact mechanism for cononsolvency has been theoretically elucidated for polymer brushes [22] and computationally simulated for polymer networks [23]. Complexities and multifaceted issues revealed from these investigations have in turn renewed a great interest in the realm of cononsolvency.

In this paper, we explore the cononsolvency behavior of PNIPAM microgels in aqueous dimethylformamide (DMF) solutions. The chaotropic effect of DMF in aqueous PNIPAM solutions has been recently classified [13], indicating that DMF is supposed to break hydrogen-bonding networks of bulk water [13,16]. Two PNIPAM chain lengths between crosslinks are used to represent relatively flat and curved chain surfaces exposed to aqueous DMF bulk solutions [24]. Our paper pursues two main issues, which to our knowledge have not been well understood. First, based on our experimental results, we characterize concentration and temperature dependences of cosolvent DMF adsorption bridging and partitioning, which allows us to quantitatively correlate the driving force with the reentrant transition of PNIPAM microgels. Second, we investigate the DMF cononsolvency effect on the persistence length of PNIPAM chains by considering the features of microgels, including the elasticity, spatial constraints, and surface charges.

The remainder of this paper is organized as follows. In Sec. II, sample preparation and characterization are presented. Analysis and discussion of the experimental data are given in Sec. III, where we follow some underlying concepts and approaches to quantitatively reveal the DMF cononsolvency effect on the PNIPAM microgel. A summary is provided in Sec. IV.

II. EXPERIMENT

A. Materials

N-isopropylacrylamide (NIPAM, 99%), *N,N'*-methylenebis (acrylamide) (BIS, 99%), potassium peroxydisulfate (KPS, 99%), *N,N*-dimethylformamide (DMF, 99.8%), and sodium dodecyl sulfate (SDS, 98%) were purchased from Sigma-Aldrich. NIPAM was dissolved in toluene (~1 g/mL) at 50 °C and the solution was placed on an ice bath. The mixed solvent of hexane and toluene (3:1 by volume) was stepwise dropped to the solution. The solution was filtered and rinsed with hexane and the recrystallized NIPAM was dried under nitrogen for about two days. BIS and KPS were purified by recrystallizing from methanol. SDS and DMF were used as received without further purification. Milli-Q grade distilled deionized water was used for the experiments.

B. Microgel preparation

PNIPAM microgels were prepared by free radical copolymerization of NIPAM and BIS using the previously reported protocol [4,25]. Briefly, the recrystallized NIPAM (6 g) and SDS (0.064 g) were dissolved in 350 mL of Milli-Q water in a 1-L three-neck round-bottomed flask fitted with a condenser, a nitrogen inlet, and a stirrer. The flask was immersed in a water bath. The solution was stirred at 200 rpm with nitrogen bubbling for 30 min at room temperature and then the temperature of the water bath was raised to 343 K. When the flask was equilibrated at 343 K, a measured amount of BIS (molar ratios of BIS to NIPAM are $f = 0.034$ and 0.0049) dissolved in 30 mL of Milli-Q water was added to the solution. After 10 min of mixing, KPS dissolved in 20 mL of Milli-Q water was added to initiate the copolymerization. The reaction proceeded at 300 rpm for 6 h. Resulting microgels were filtered and purified by successive centrifugation, decantation, and redispersion in Milli-Q water. Microgels were further dialyzed against the Milli-Q water for one week with three changes of water per day. Solid contents of final microgels were estimated by free drying to be 3.7 and 5.4%, respectively, for the molar ratios $f = 0.034$ and 0.0049.

C. Microgel size

The hydrodynamic radius R_h of PNIPAM microgels was measured by dynamic light scattering (DLS). Measurements were performed on a Malvern 4700c apparatus equipped with

a correlator and an argon ion laser operating at a wavelength of 488 nm. The spectrometer was calibrated using the distilled water to make sure that the scattering intensity from water had no angular dependence. The experimental correlation function was measured and analyzed with the built-in routine. R_h was calculated from the first cumulant of the correlation function using the Stokes-Einstein approximation. The temperature was controlled with an accuracy of ±0.1 K. The microgel dispersion was diluted to about 10^{-5} g/g with mixed solvents of Milli-Q water/DMF for DLS measurements. Samples were thermally equilibrated for 20 min prior to measurements. A stream of dry nitrogen blew through the sample chamber to prevent possible moisture condensation at lower temperatures. The measurements were repeated at least six times for each sample.

D. Chain parameters

In order to give a quantitative description of cononsolvency, it is necessary to have two key parameters characterizing chains of the PNIPAM microgel: the number of crosslinked chains, $N_{\rm ch}$, and the number of monomers between two crosslinks, N_l. Unfortunately, a direct measurement of N_l or $N_{\rm ch}$ is experimentally inaccessible. As such, we calculate the chain parameters utilizing temperature-dependent data of the PNIPAM microgel in pure water [Fig. 2(a)].

The number of crosslinked chains in the microgel, $N_{\rm ch}$, is given by [26]

$$N_{\rm ch} = \frac{2V_{hr}\phi_{pr}\rho_p N_A f}{M} \tag{1}$$

where $\rho_p = 1.1\,{\rm g/cm^3}$ is the density of PNIPAM, N_A is the Avogadro constant, $M = 113$ is the molecular weight of the monomer, and V_{hr} and ϕ_{pr} are the microgel volume V_h and polymer volume fraction ϕ_p in pure water of the reference state, respectively. V_{hr} is calculated from the experimental data at $T = 333\,{\rm K}$ [Fig. 2(a)]. The polymer volume fraction ϕ_p is given by $\phi_p = \phi_{pr}V_r/V_h$. Note that in the literature the value of the reference state ϕ_{pr} for PNIPAM microgels is usually varied between 0.7 and 0.85 although a lower value was recently reported [26]. In this paper, the average value of $\phi_{pr} = 0.8$ is taken as the reference state [26]. The size of PNIPAM microgels is essentially independent of molar ratio f studied when $T > 323$ K. The average number of monomers per chain between two crosslinks, N_l, is obtained by

$$N_l = \frac{3V_{hr}\phi_{pr}}{4\pi a^3 N_{\rm ch}} \tag{2}$$

where a is the monomer size of 3 Å corresponding to two collinear C-C bonds. Our calculations yield $N_{\rm ch} = 8.2\times10^5$ and $N_l = 22$ for molar ratio $f = 0.034$ and $N_{\rm ch} = 1.2\times10^5$ and $N_l = 150$ for molar ratio $f = 0.0049$, which will be invoked later in the discussion of the cononsolvency phenomenon of PNIPAM microgels in the aqueous MDF.

Here we utilize them to estimate the interaction parameter between polymer and solvent in pure water χ [26]:

$$\chi(\phi_p) = \frac{1}{\phi_p^2}\left\{\frac{N_{\rm ch}\nu_s}{V_{hr}N_A}\left[\frac{\phi_p}{2\phi_{pr}} - \left(\frac{\phi_p}{\phi_{pr}}\right)^{1/3}\right] - \phi_p - \ln(1-\phi_p)\right\} \tag{3}$$

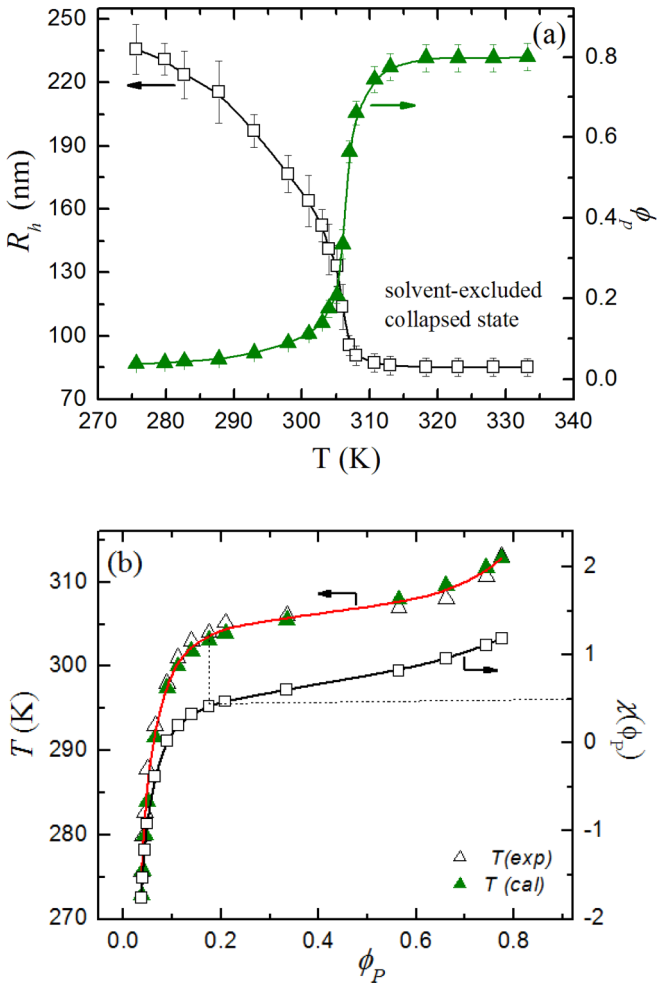

FIG. 2. (a) Hydrodynamic radius R_h and polymer volume fraction ϕ_p with molar ratio $f = 0.034$ as a function of temperature in pure water. (b) Temperature and interaction parameter χ of PNIPAM microgel as a function of ϕ_p in pure water.

where ν_s is the mole volume of water. The results are shown in Fig. 2(b) as a function of ϕ_p. Temperatures at which the osmotic pressures of water inside and outside the PNIPAM microgel become equal are also calculated by [27]

$$T = \frac{AT_{\rm LCST}\phi_p^2}{\frac{N_{\rm ch}\nu_s}{V_{hr}N_A}\left[\frac{\phi_p}{2\phi_{pr}} - \left(\frac{\phi_p}{\phi_{pr}}\right)^{1/3}\right] - \phi_p - \ln(1-\phi_p) + \left(A-\frac{1}{2}\right)\phi_p^2 - C\phi_p^3} \tag{4}$$

where A and C are entropy- and composition-dependent parameters, respectively, but they are usually treated as fitting parameters. For the PNIPAM microgel with $f = 0.034$, the best fit gives $A = -19.5$ and $C = 0.25$. Figure 2(b) shows that $\chi = 0.5$ is obtained at $\phi_p \approx 0.18$ corresponding to $T \approx 304\,{\rm K}$, which indicates a good agreement between the calculated results and the experimental data.

III. RESULTS AND DISCUSSION

A. Reentrant transition

The hydrodynamic radius R_h of PNIPAM microgels is presented in Fig. 3 as a function of DMF mole fraction x_c. The

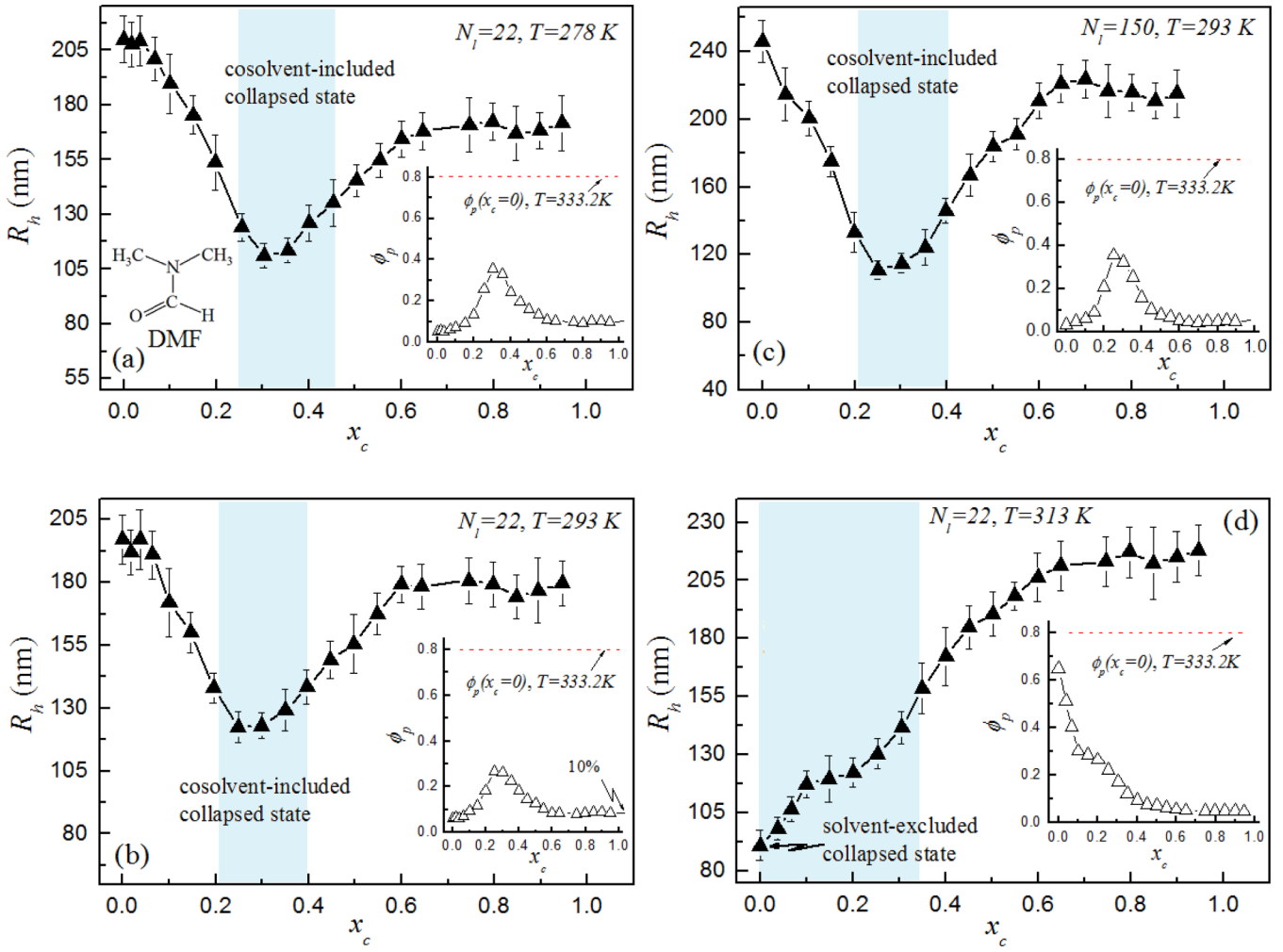

FIG. 3. Hydrodynamic radius R_h as a function of x_c. Shadow areas are two-phase regions of linear PNIPAM at indicated temperatures [10]. Insets show polymer volume fraction ϕ_p as a function of x_c. Error bars of ϕ_p are smaller than the size of symbols.

results show the swelling-to-collapse transition in the water-rich region, followed by the collapse-to-reswelling transition. In greater detail, at 278 K, the size of the microgel with $N_l = 22$ is 210 nm at $x_c = 0$ and the addition of a very small amount of DMF does not affect the size [Fig. 3(a)]. The microgel undergoes the collapse transition monotonically with increasing x_c until a threshold $x_c^* \approx 0.3$ is reached corresponding to the minimum size $R_h^{\min} = 110$ nm. As x_c is further increased, the microgel swells to a plateau of $R_h^{\text{plat}} \approx 170$ nm in the range $x_c > 0.6$.

When temperature is increased to $T = 293$ K, the size of the microgel is slightly reduced to 200 nm in water [Fig. 3(b)]. The reentrant transition shows the larger $R_h^{\min} \approx 122$ nm at the lower $x_c^* \approx 0.25$ and the larger $R_h^{\text{plat}} \approx 180$ nm in the range $x_c > 0.6$. The characteristic sizes $R_h^{\min}$ and R_h^{plat} at $T = 293$ K are larger than those at $T = 278$ K, as are their swelling ratios $R_h^{\min}/R_h(x_c = 0)$ and $R_h^{\text{plat}}/R_h(x_c = 0)$. The size of the PNIPAM microgel with $N_l = 150$ is presented in Fig. 3(c) at 293 K. The reentrant transition shows that the size is reduced from 245 nm in water to $R_h^{\min} \approx 110$ nm at $x_c^* \approx 0.25$ and increased to $R_h^{\text{plat}} \approx 220$ nm at $x_c > 0.6$. Compared with $N_l = 22$, the microgel with $N_l = 150$ is collapsed to the smaller $R_h^{\min}$ but reswollen to the larger R_h^{plat}. Note that in all the cases the sizes of microgels in the vicinity of pure DMF are smaller than those in pure water.

For the purpose of comparison, the effect of DMF on the PNIPAM microgels is presented at $T > T_{\text{LCST}}$ [Fig. 3(d)]. At 313 K, the microgel with $N_l = 22$ is collapsed to a compact structure of 90 nm in pure water. The addition of DMF triggers the swelling transition of the already collapsed microgel. It is worth noting that the swelling transition exhibits a plateau within the regime where linear PNIPAM chains undergo the phase separation [10]. This behavior may be associated with the formation of small clusters during the progressive dissolution of the collapsed microgel while the overall size of the microgel remains essentially unchanged [28]. Considering that at $T > T_{\text{LCST}}$ the cosolvent-strived expansion is strongly constrained by temperature-induced collapse, it is not impossible that some intermediate structures of the collapsed microgel can exist as a balance of the competition between expansion and collapse. With increasing x_c, the microgel continuously swells and eventually equilibrates at a plateau when $x_c > 0.65$. It is particularly notable that the plateau size of $R_h^{\text{plat}} \approx 215$ nm at $T > T_{\text{LCST}}$ is larger than the sizes in

TABLE I. Hansen solubility parameters ($MPa^{1/2}$) for DMF, water, and PNIPAM.

Compounds	δ_T (total)	δ_D (dispersion)	δ_P (polar)	δ_H (hydrogen bond)
DMF[a]	24.8	17.4	13.7	11.3
Water[a]	47.8	15.5	16.0	42.3
PNIPAM[b]	22.1	16.7	12.7	7.0

[a]Solubility parameters are taken from [30].
[b]Solubility parameters are calculated from group contributions [30].

pure water at $T < T_{\mathrm{LCST}}$. Obviously, the results demonstrate that at $T > T_{\mathrm{LCST}}$ the solvent quality of DMF-water mixtures becomes increasingly better for the PNIPAM microgel with increasing DMF concentration.

The polymer volume fraction ϕ_p is shown in the insets of Fig. 3 as a function of x_c. Apparently, all the maximum ϕ_p values of the cononsolvency-induced collapse are much smaller than that of the temperature-induced collapse, showing the distinct feature of the solvent-included collapsed state. Our results are consistent with the partially collapsed PNIPAM microgels obtained from a combination of small angle neutron scattering and neutron spin echo spectroscopy [29]. It is worth noting that the monomer density of PNIPAM microgels exhibits a parabolic distribution [29], analogous to polymer brushes. Specifically, at the same $x_c(=0.2)$, the ϕ_p values of this paper are comparable to the medium ϕ_p value obtained from the methanol-water mixture [29].

Three issues are often concerned with the cononsolvency phenomenon: (i) the relative cosolvent quality for the polymer, (ii) the cononsolvency mechanism, and (iii) the cosolvent-included collapsed state. For the first issue, the detailed description shall be given later. Here we would first like to use the Hansen solubility parameter δ_T as a heuristic guide to assess the relative molecular affinity of DMF to PNIPAM [30]. Hansen solubility parameter δ_T comprises three components representing dispersion δ_D, polar δ_P, and hydrogen bond δ_H interactions (Table I). Compared with water, the Hansen solubility parameters of DMF are all closer to those of PNIPAM. It is generally accepted that the affinity between a polymer and a solvent will be maximized when their solubility parameters are optimally matched [30].

For the cononsolvency phenomenon of PNIPAM, recent investigations have experimentally revealed that crosslinking or bridging of urea [11,16] and methanol [14,15] to PNIPAM chains is the driving force for the conformational collapse of PNIPAM. These findings have lent credence to the theoretical and computational studies regarding the direct contact mechanism for cononsolvency [18,19,22,23]. When considering the DMF chemical structure, the preferential adsorption bridging in the current system is involved in the hydrogen bonding and hydrophobic interactions between DMF and PNIPAM, analogous to the bivalent binding of urea [11,16] and methanol [14,15] with PNIPAM. For example, the hydrogen group of DMF can be hydrogen bonded with the amide group of NIPAM, whereas the methyl group of DMF can interact with the isopropyl group of NIPAM. It is worth noting that the bridging of cosolvent molecules to a polymer is highly cooperative [11,16] and can be implemented through a collective effect of several cosolvent molecules between adjacent chains [14,15,18]. The amount of DMF bridging adsorption to the PNIPAM chain will be quantitatively described in the next section.

Cononsolvency leads to the cosolvent- or solvent-included collapsed state at $T < T_{\mathrm{LCST}}$, which is distinct from the conventional collapse at $T > T_{\mathrm{LCST}}$ where solvent molecules are progressively excluded from the chain surface under poor solvency. These two collapsed states are contrasted by the polymer volume fraction ϕ_p (Fig. 3, insets). In particular, the maximum ϕ_p of the cosolvent- or solvent-included collapsed state at $T < T_{\mathrm{LCST}}$ is smaller than one half of the maximum ϕ_p of the solvent-excluded collapsed state at $T > T_{\mathrm{LCST}}$. Obviously, the former is a loosely collapsed structure whereas the latter is a densely packed globule. The amount of cosolvent or solvent in the cononsolvency-induced collapsed state will be determined later. In all the cases, ϕ_p at the maximally swollen state is around 0.05–0.1, depending on temperature.

B. Adsorbed amount of the cosolvent or solvent

The preferential adsorption bridging of cosolvent molecules to polymer chains leads to the effective monomer-monomer attraction driving the conformational collapse at $T < T_{\mathrm{LCST}}$ [11,18,19,22,23]. Quantitative description of cosolvent or solvent molecules adsorbed to (or repelled from) individual polymer chains has long remained challenging. In a multicomponent system, the conformational transitions further complicate the characterization. For polymer networks, it is also difficult to explicitly get an analytical expression for the total number of adsorbed cosolvent or solvent molecules due to a random distribution of crosslinked chains throughout polymer networks.

To circumvent the difficulties, we consider a microgel consisting of N_{ch}/p cells of p chains (Fig. 1). Assume that the unit cell is a bcc of eight chains ($p = 8$) [31] with a contour length $L_C = aN_l$. Here a constrained chain is considered semiflexible because its bending stiffness is large enough such that its bending energetics can just surpass the entropy of contracting the whole chain toward a random coil. The radius of the microgel and the volume fraction of the polymer can be approximated by $R_h \approx (N_{\mathrm{ch}}/8)^{1/3}R_{ee}$ and $\phi_p \approx 8a^3N_l/{R_{ee}}^3$, respectively, where R_{ee} is the end-to-end distance between the crosslinks. Semiflexible chains are described by the wormlike chain (WLC) model [32], where the end-to-end distance is related to two length scales: contour length L_C and persistence length l_p. In this paper, the cononsolvency effect on PNIPAM microgels is also pertinent to other parameters such as bridge constraints, surface charges, and conformational transitions. Little is known about the chain behavior of PNIPAM microgels under the interplay of these complicated factors in cononsolvency. We shall discuss this issue in detail later.

Now when viewed from an individual chain, there are N_l sites exposed to the bulk solution of mixed solvents. Among them, n_C^A sites are occupied by the nonbridging adsorption of cosolvent molecules, n_C^B sites are occupied by the bridging adsorption, and n_S sites are occupied by solvent (water) molecules. Alternatively, using the denotation of the mole fraction, we have $\phi_A + \phi_B + \phi_S = 1$ with $\phi_A = n_C^A/N_l$,

$\phi_B = n_C^B/N_l$, and $\phi_S = n_S/N_l$. In such a multicomponent system, the polymer is considered as an adsorbing substrate to which the solvent and cosolvent compete to adsorb in the course of the cononsolvency effect. The free energy for the preferential adsorption and bridging can be written as

$$f_{\text{ads. brid.}} = \phi_A \ln \phi_A + \phi_B \ln \phi_B + (1-\phi_A-\phi_B)\ln \times (1-\phi_A-\phi_B) - \varepsilon_A\phi_A - \varepsilon_B\phi_B - \frac{\mu_c}{k_BT}(\phi_A+\phi_B) \tag{5}$$

where $f_{\text{ads. brid.}} = F_{\text{ads.brid.}}/N_l N_{\text{ch}}$ is the free energy per monomer unit; ε_A and ε_B are the parameters characterizing the nonbridging and bridging adsorption energies of cosolvent molecules, respectively; and $\mu_c = k_BT \ln[x_c/(1-x_c)]$ [22] is the chemical potential of the cosolvent in the bulk solution. The free energy is taken in units of k_BT throughout this paper. The first three terms account for entropies of all the possible arrangements of the adsorption. The energy $\varepsilon_i\phi_i$ describes interactions of the cosolvent with the polymer. Notably, for polymer networks, the bridging adsorption of cosolvent molecules refers to the attraction of monomers between different chains. Compared with a free chain [18], looping a constrained chain by cosolvent bridges is energetically unfavorable and thus not taken into account, analogous to the theoretical work of polymer brushes in mixtures of two solvents [22]. At $T > T_{\text{LCST}}$, the cononsolvency phenomenon does not exist [12,15], as observed from the results in Fig. 3(d), and thus $\phi_B = 0$. A combination of all-atom simulations, generic simulations, theoretical analysis, and nuclear magnetic experiments has shown a general consensus regarding the relation between polymer dimension and cosolvent concentration, yielding the mole fraction of the bridging adsorption in the equilibrium state [14,18]:

$$\phi_B(x_c) = \frac{[R_{ee}(x_c)/R_{ee}(x_c=0)]^{-3}-1}{N_l} = \frac{[R_h(x_c)/R_h(x_c=0)]^{-3}-1}{N_l}. \tag{6}$$

In the unit cell, the cosolvent bridging most likely initiates from sites closer to the crosslink and radially develops outward due to a parabolic distribution of monomer density [29]. Every bridge formed consequently leads to the smaller distance between the chains, which can provide the bridging opportunity for succeeding cosolvent molecules.

An analytical approach is hampered by difficulties in determining the parameter ε_i involving different types of interactions in such a multicomponent system. As a first approximation, we utilize the Hansen solubility parameter, a global effect characterizing interactions in multiple components, to estimate the energy of the cosolvent bridging adsorption:

$$\varepsilon_B = \frac{2\upsilon_c}{zk_BT}\delta_{T,P}\delta_{T,C}\phi_p = \varepsilon_0\phi_p \tag{7}$$

where υ_c is the mole volume of the cosolvent, $z = 6$ is the number of nearest neighbors per monomer for the cubic geometry [33], and $\delta_{T,P}$ and $\delta_{T,C}$ are Hansen solubility parameters of polymer and cosolvent, respectively (Table I). δ_T is related to its three components by $\delta_T = \sqrt{\delta_D^2+\delta_P^2+\delta_H^2}$ [30]. In this simplified approach, the hydrogen bonding component δ_H is actually utilized to account for any other interactions which are not included in the components δ_D and δ_P. Within the framework of the mean-field attraction, the average probability that the cosolvent is in contact with the chain through the hydrogen bonding is assumed to be the same as that through the hydrophobic interaction. Minimization of the free energy with respect to ϕ_A leads to an analytical expression:

$$\phi_A(x_c) = \frac{x_c \exp(\varepsilon_0\phi_p/2)(1-\phi_B)}{1+x_c\exp(\varepsilon_0\phi_p/2)}. \tag{8}$$

The cononsolvency phenomenon is quantitatively related to the amount of the adsorbed DMF molecules (Fig. 4). For $N_l = 22$, the mole fraction of the bridging adsorption ϕ_B is not affected by temperature in the collapse region of $x_c < 0.25$ [Fig. 4(a)]. The maximum ϕ_B decreases from 0.26 at 278 K to 0.15 at 293 K, indicating the increase in the mixed solvent quality at the higher temperature. In the reswelling transition, ϕ_B decreases with x_c as expected but the cosolvent bridges do not totally vanish once they form. Specifically, when viewed from the microgel as a whole, the total number of cosolvent bridges $\phi_B N_l N_{\text{ch}}$, for instance, is around 3.5×10^6 in the plateau region where ϕ_B is 0.04 for $N_l = 22$ at 273 K. The results rationalize the experimental observation that the plateau size of the microgel is smaller than that in water at $T < T_{\text{LCST}}$, despite the better affinity of DMF to PNIPAM. By contrast, at $T > T_{\text{LCST}}$ where cononsolvency does not exist, the size of the microgel is eventually larger than the size in pure water [Fig. 3(d)]. Note that the explanation for why there is no cononsolvency effect at $T > T_{\text{LCST}}$ is unclear to date, which may be associated with chain packing effects and a repulsion-by-attraction mechanism [19].

The mole fraction of nonbridging adsorption ϕ_A exhibits a continuous increase with x_c [Fig. 4(b)]. This behavior manifests a good solvency for PNIPAM segments enriched by sticky contacts of DMF molecules. The increase in ϕ_A is faster in the collapse transition than that in the reswelling transition. In particular, for the maximally collapsed state, ϕ_A is about twice as large as ϕ_B at 278 K and about 3.5 times larger than ϕ_B at 293 K, indicating the temperature dependence of the nonbridging adsorption in the cosolvent-included collapsed state. The results also indicate that the longer chain has the higher mole fraction of nonbridging adsorption within the range of the collapsed transition. It is particularly notable that for the longer chain ϕ_A is not changed much between $x_c \approx 0.25$ and 0.4, corresponding to the range where the maximum of the collapse transition is achieved. Considering that the cosolvent bridge can be cooperatively implemented through a collective effect of several cosolvent molecules [14,15,18], the results imply that for the larger distance between the chains some of the adsorbed DMF molecules will be involved in the cosolvent bridging process. In this case, ϕ_B increases with x_c while ϕ_A remains roughly unchanged. At $x_c > x_c^{\min}$, where the bridge adsorption is displaced by the nonbridge adsorption, the increase in ϕ_A is essentially independent of temperature and chain length. Taken all together, since the molecular affinity of DMF to the PNIPAM microgel gets increasingly better with the DMF concentration, the conformational collapse is considered to decouple from the solvent quality of DMF-water mixtures. The results are consistent with theoretical

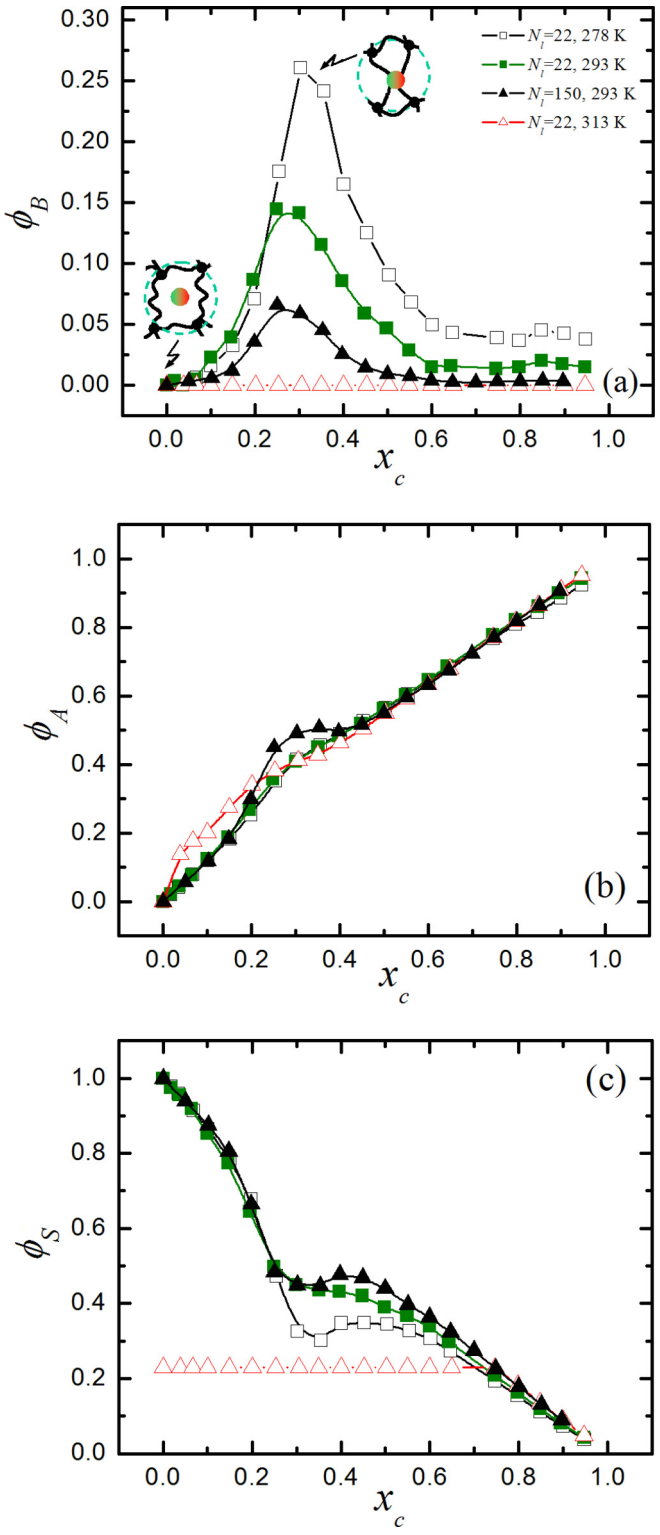

FIG. 4. Adsorbed mole fractions per chain ϕ_i as a function of x_c: (a) mole fraction of cosolvent bridge adsorption ϕ_B, (b) mole fraction of cosolvent nonbridge adsorption ϕ_A, and (c) mole fraction of solvent or water adsorption ϕ_S.

work [18,22,23] and experimental observations [11,14,15], which indicates that the DMF-induced collapse of PNIPAM microgels is not a conventional collapse under poor solvent conditions.

The results show that the variation of ϕ_S with x_c proceeds through three stages. It can be seen from Fig. 4(c) that ϕ_S decreases quickly in the range of $x_c < 0.3$, corresponding to the sharp increase in both ϕ_B and ϕ_A. In this collapse regime, more than half of the adsorbed water molecules are eventually expelled from the surface of polymer chains, depending on T. Then, ϕ_S tends to be roughly steady in the range between $x_c \approx 0.3$ and 0.5, which depends on both T and N_l. In this reswelling regime, the steady water amount on the polymer surface is attributed to the balance between the decrease of ϕ_B and the increase of ϕ_A. Finally, as x_c is further increased, water is progressively displaced by DMF nonbridging adsorption, irrespective of T and N_l. The analysis again shows the better affinity of DMF to PNIPAM in competing with water.

At $T > T_{\mathrm{LCST}}$, the addition of DMF triggers the swelling of densely packed microgels which otherwise effectively expel water molecules from the chain surface [Fig. 4(c)]. There are two steps for the swelling transition at $T > T_{\mathrm{LCST}}$: (i) the preferential adsorption of DMF to unoccupied sites of PNIPAM chains and (ii) the displacement of already adsorbed water by DMF. In the first step, the water content remains unchanged in a broad range of x_c until the unoccupied sites are saturated with DMF molecules. In the second step, the adsorbed water is displaced by DMF as x_c is further increased.

C. Cosolvent partitioning

While the preferential adsorption bridging of DMF to PNIPAM induces the conformational collapse of PNIPAM microgels, as shown in the preceding section, a large amount of DMF molecules are eventually incorporated into the collapsed structure at $T < T_{\mathrm{LCST}}$, which is distinct from the conventional collapse of PNIPAM at $T > T_{\mathrm{LCST}}$. In this case, the distribution of cosolvent molecules between the chain surface and bulk solution can be quantified by the local-bulk partitioning model [34], which has been used to account for the cosolvent effect on protein stability [35]. In spite of the fact that the cosolvent-induced polymer collapse is distinct from the cosolvent-protected native (folded) proteins, both comply with the thermodynamic description for the preferential binding of cosolvents with chain molecules.

In the simplest form, the local-bulk partition coefficient K_p is given by [34]

$$K_p(x_c) = \frac{(n_C/n_S)^{\mathrm{local}}}{(n_C/n_S)^{\mathrm{bulk}}} \tag{9}$$

In general, the local domain is defined by the total number of cosolvent molecules at the chain surface. $K_p > 1$ identifies the excess number of cosolvent molecules in the local domain and thus characterizes the molecular affinity of cosolvent molecules to chain molecules, whereas $0 < K_p < 1$ indicates the preferential exclusion of cosolvent molecules from the chain surface. In this paper, considering the conformational collapse driven by the cosolvent bridge, the local-bulk partition coefficient for the bridge adsorption, K_p^B, is also taken into account. The number of DMF molecules in the local domain can be seen from Fig. 5.

The preferential adsorption of DMF molecules is clearly evidenced from the remarkable increase in the coefficient K_p [Fig. 6(a)]. The variation of K_p with x_c is not significantly

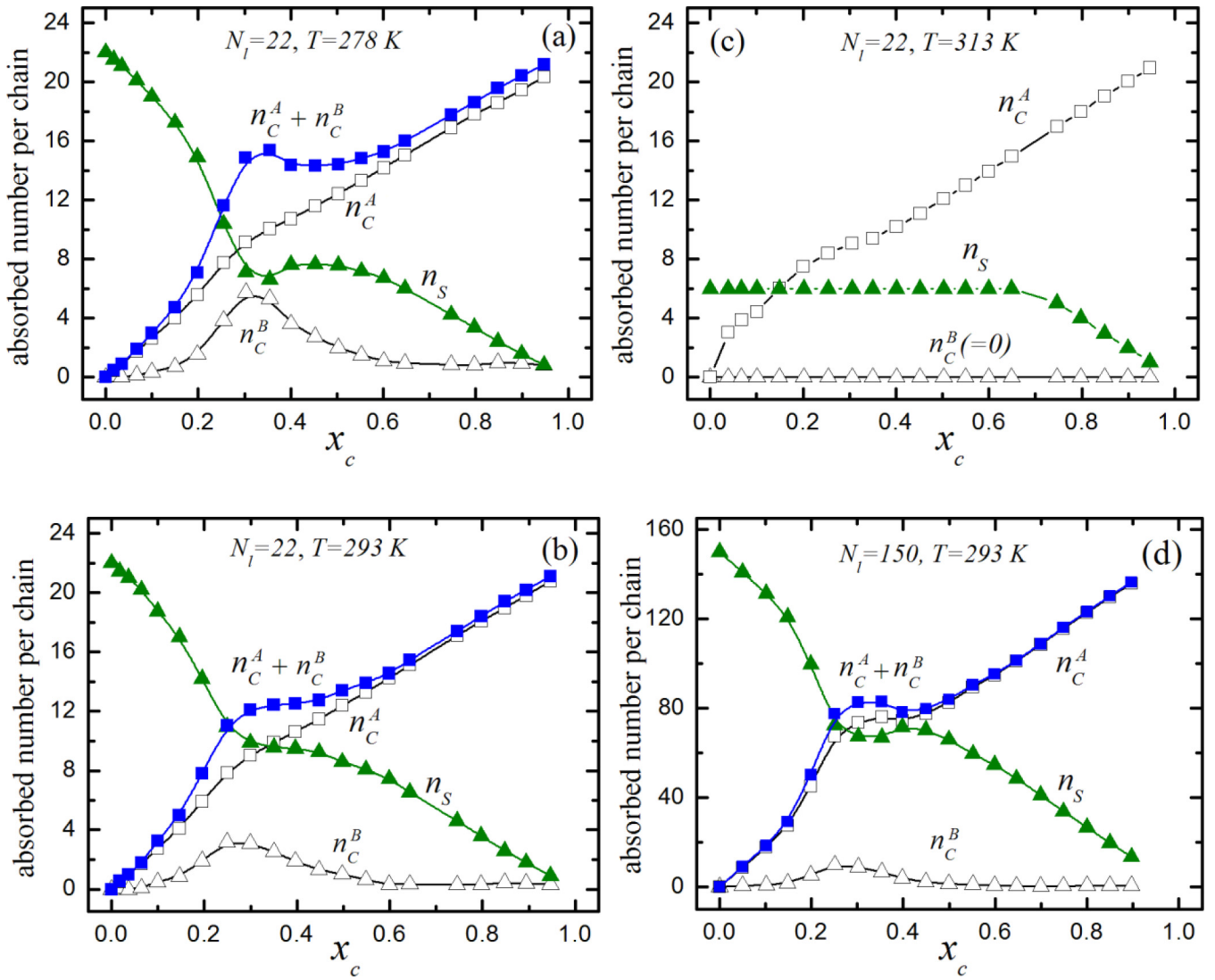

FIG. 5. Absorbed number of cosolvent or solvent per chain as a function of x_c.

affected by temperature and chain length during the collapse transition at $x_c < x_c^*$. The peak value of K_p at 278 K is much larger than that at 293 K but essentially independent of chain length. When $x_c > x_c^*$, the coefficient K_p decreases with the reswelling transition and eventually reaches a thermodynamically equilibrium state in the plateau region. By comparison, the partition coefficient for the bridge adsorption K_p^B manifests the stronger dependence of chain length [Fig. 6(a), inset]. It can be seen that at 293 K the coefficient K_p^B for $N_l = 22$ is larger than that for $N_l = 150$ in the entire range of the DMF concentration.

We also consider the preferential binding parameter ν_{pc} characterizing the competitive binding between DMF and water. In the limit of very dilute concentrations so that the interaction between microgels can be ignored, the preferential binding parameter, ν_{pc}, is defined by [35,36]

$$\nu_{pc}(x_c) = -\left(\frac{\partial \mu_p}{\partial \mu_c}\right)_{P,T,\rho_p} = n_C(x_c) - \frac{\langle n_c \rangle}{\langle n_s \rangle} n_S(x_c) = n_C(x_c)\left(1 - \frac{1}{K_p(x_c)}\right) \quad (10)$$

where μ_p is the chemical potential of the polymer at pressure P. Upon the occurrence of cononsolvency, the change of the preferential binding parameter, $\Delta\nu_{pc}$, is given by [36]

$$\Delta\nu_{pc}(x_c) = -\left(\frac{\partial \Delta\mu_p}{\partial \mu_c}\right)_{P,T,\rho_p} = \Delta n_C(x_c) - \Delta\left(\frac{n_C(x_c)}{K_p(x_c)}\right) \quad (11)$$

where $\Delta\mu_p = \mu_p(x_c) - \mu_p(x_c = 0)$ with respect to pure water of the reference state. In the equilibrium state, $\Delta\nu_{pc}$ can be positive, negative, or zero. A positive value thermodynamically favors the preferential adsorption or interaction between cosolvent molecules and the polymer chain surface, whereas a negative value favors the exclusion of cosolvent molecules from the polymer chain surface. $\Delta\nu_{pc} = 0$ means that the interaction between cosolvent molecules and the polymer chain surface is thermodynamically not different from the reference state.

The normalized preferential binding parameter $\Delta\nu_{pc}/N_l$ is shown in Fig. 6(b) as a function of x_c, as complimentary to the partition coefficient K_p. The values of $\Delta\nu_{pc}$ are positive with respect to pure water, thereby rendering the thermodynamic

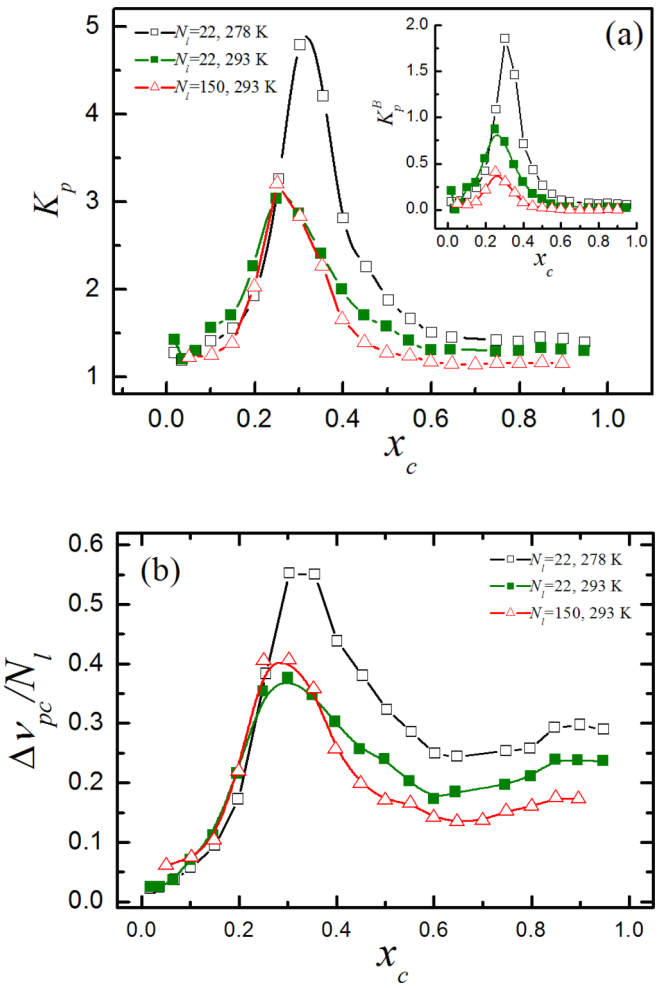

FIG. 6. Local-bulk partition coefficient K_p (a) and normalized preferential binding parameter ν_{pc}/N_l (b) as a function of x_c.

driving force to transfer DMF molecules from the bulk solution to the PNIPAM chain surface. Moreover, it is helpful to note that the values of $\Delta\nu_{pc}/N_l$ are notably distinct from the reference state in the DMF-rich region. Thus, as compared with K_p, the results of $\Delta\nu_{pc}/N_l$ explicitly indicate that DMF is always in excess at the chain surface and the excess is dependent on temperature and chain length in the DMF-rich region [Fig. 6(b)]. Taken all together, thermodynamically favorable states involve the preferential binding of DMF molecules with PNIPAM microgels in collapsed and reswollen states, which rationalizes the experimental results concerning the cononsolvency effect.

D. Cononsolvency effect on chain flexibility

In pure water, PNIPAM microgels have intriguing mechanical properties in response to the variation of temperature [2]. They manifest the softening behavior in the vicinity of T_{LCST} [37,38] and become increasingly stiffer at $T > T_{\mathrm{LCST}}$ [39–41]. The stiffness behavior is also found from interfacial PNIPAM in the presence of cosolvents [42] and surfactant micelles [43].

Motivated by the previous studies, we are concerned with the DMF cononsolvency effect on the chain flexibility of PNIPAM microgels. The investigation is of interest from two points of view. First, since cononsolvency occurs at $T < T_{\mathrm{LCST}}$, understanding the cononsolvency effect on the chain flexibility is a step toward the universality of stimuli-responsive chain flexibility. Second, the cononsolvency effect on mechanical properties of polymers is of practical interest in a broad range of applications at $T < T_{\mathrm{LCST}}$.

We put forward a thermodynamic approach to describe the cononsolvency effect of DMF on PNIPAM microgels. The analysis involves four elements characterizing the free energy per chain of a microgel, f_M, in a mean-field approximation:

$$f_M = f_{\mathrm{ads.brid.}} + f_{\mathrm{elas}} + f_{\mathrm{conf}} + f_{\mathrm{elec}}. \tag{12}$$

The first term, $f_{\mathrm{ads.brid.}}$, has been given in Eq. (5). The second term, f_{elas}, in Eq. (12) accounts for the elastic free energy of semiflexible chains, which can be expressed as a function of the end-to-end distance [44]:

$$f_{\mathrm{elas}} = \frac{\pi^2 l_p}{2L_C}\left[1 - \left(\frac{R_{ee}}{L_C}\right)^2\right] + \frac{2L_C}{\pi l_p[1-(R_{ee}/L_C)^2]}. \tag{13}$$

Note that Eq. (13) is also valid to characterize other situations regarding the chain flexibility if specific conditions are fulfilled [44].

The third contribution, f_{conf}, in Eq. (12) corresponds to the free energy of polymer chains under confinements in microgel networks, which is approximated by [45]

$$f_{\mathrm{conf}} = \frac{a\pi^2 L_C}{16{R_{ee}}^2} - \frac{1}{8}\ln V_c \tag{14}$$

where the volume V_c is associated with the cononsolvency effect. The first term in Eq. (14) reflects the fact that the constrained chains are far more rigid to bending than free chains. The volume $V_c = 4\pi{\xi_B}^3/3$ takes into account the cosolvent bridge with ξ_B being the average mesh size of bridges. ξ_B can be approximated by $\xi_B \approx (6/\pi\rho_B)^{1/3}$ [46] with the number density of cosolvent bridges $\rho_B \approx N_{\mathrm{ch}} n_C^B/(4\pi{R_h}^3/3)$. The bridge adsorption of cosolvent molecules enhances the already existing restraints in microgel networks and as a consequence reduces f_{conf}.

The last term, f_{elec}, in Eq. (12) represents the electrostatic free energy of surface charges of microgels. The neutral PNIPAM is electrostatically charged due to the utilization of an ionic initiator for the microgel preparation. Since the polymerization was carried out at 343 K, the globular PNIPAM should force the charges toward the aqueous solution to form a charge corona on the microgel surface [47]. In general, for a uniformly charged particle having radius r, charge density ρ_E, and total charge q, a charge has an electrostatic potential $\Gamma(r) = q(r)/4\pi\varepsilon_0\varepsilon r$ at r, where ε_0 is the dielectric constant of the vacuum and ε is the dielectric constant of the solvent (water). As such, the free energy of microgels is

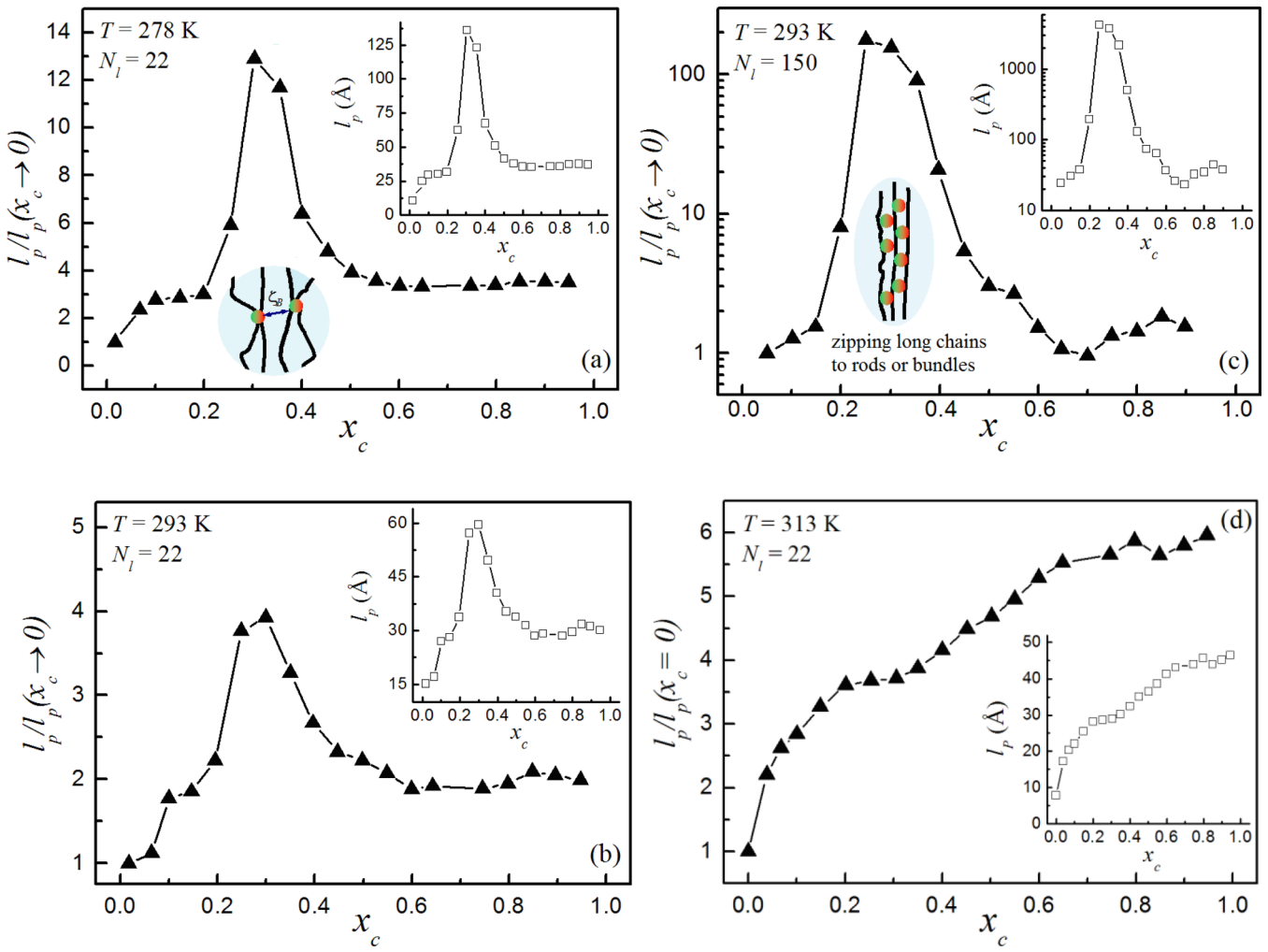

FIG. 7. Relative persistence length $l_p/l_p(x_c = 0)$ and persistence length l_p (insets) as a function of x_c.

given by

$$f_{\text{elec}} = \frac{1}{k_B T N_l N_{\text{ch}}} \int_0^{R_h} \Gamma(r) dq = \frac{1}{k_B T N_l N_{\text{ch}}} \int_0^{R_h} \frac{q(r)}{4\pi\varepsilon_0 \varepsilon r} dq. \tag{15}$$

The charge density ρ_E and total charge $q(r)$ can be given by $\rho_E = eZ_{\text{eff}}/4\pi {R_h}^2$ and $q(r) = 4\pi r^2 \rho_E$, respectively, where Z_{eff} is the number of the effective surface charge and e is the elementary charge. Substituting ρ_E, $q(r)$, and $dq = 8\pi r \rho_E dr$ into Eq. (15) and then integrating over r up to R_h, we have the free energy f_{elec}:

$$f_{\text{elec}} = \frac{4 l_B {Z_{\text{eff}}}^2}{3 N_l {N_{\text{ch}}}^{4/3} R_{ee}} \tag{16}$$

where $l_B = e^2/4\pi k_B T \varepsilon_0 \varepsilon$ is the Bjerrum length. The effective surface charge was recently found to increase with the size of PNIPAM microgels and the corresponding number of effective surface charges Z_{eff} can be calculated by $Z_{\text{eff}} = 198 + 50.56 {R_h}^{1/2}$ [48]. In the calculation of the Bjerrum length l_B, temperature-dependent data of dielectric constant ε can be obtained in the literature [49].

Minimization of the free energy f_M with respect to the end-to-end distance leads to an analytical expression as follows:

$$l_p = \frac{\sqrt{F^2 - 4DG} - F}{2D} \tag{17}$$

where

$$D = \pi^2 {R_{ee}}^5,$$

$$F = \frac{\pi^2 a^5 {N_l}^4 R_{ee}}{8} + \frac{3(aN_l R_{ee})^3}{8 n_C^B} - 12 a^6 {N_l}^4 \varepsilon_B (\phi_A + 2\phi_B) + \frac{4 l_B a^3 (N_l R_{ee} Z_{\text{eff}})^2}{3 {N_{\text{ch}}}^{4/3}},$$

$$G = -\frac{4(aN_l)^6 {R_{ee}}^5}{\pi[(aN_l)^2 - {R_{ee}}^2]}.$$

The persistence length l_p is shown in Fig. 7 as a function of x_c for different temperatures and molar ratios. First, to assess the analytical results, it is essential to make a comparison of the persistence length in pure water ($x_c = 0$) with experimental data in the literature. Kutnyanszky *et al.* reported $l_p \approx 4.5$–5.4 Å in different solvents at temperatures below and above T_{LCST} [50]. Ricka *et al.* reported $l_p \approx 7$–10 Å [51],

while Binkert *et al.* estimated $l_p \approx 33$ Å at 298 K, which increases with temperature [52]. Haupt *et al.* estimated $l_p \approx 4$ Å by fitting the WLC model to force-distance profiles [53]. Ahmed *et al.* found the monomer number of the persistence length is about 10 as deduced from the analysis of the PNIPAM collapse rate [54]. We are aware that the literature data vary widely, which may be attributed to system-specific conditions such as chain lengths and experimental methods. Our results show that, at $x_c \approx 0$, l_p is about 11 and 15 Å for $N_l = 22$ at 278 and 293 K, respectively. For $N_l = 150$ at $x_c \approx 0$, l_p is about 24 Å at 293 K. Additionally, at $T > T_{\mathrm{LCST}}$, the persistence length of $N_l = 22$ is about 8 Å at 313 K. Apparently, all the results obtained from pure water fall in the range of experimental values reported in the literature.

The analysis shows that, analogous to the temperature-induced stiffness of PNIPAM microgels [36–40], the DMF cononsolvency also leads to a remarkable increase in the persistence length of PNIPAM chains (Fig. 7). For instance, in the context of the maximally collapsed state where the PNIPAM chains with $N_l = 22$ are collapsed by six DMF bridges at 278 K, as shown in Fig. 5(a), the persistence length l_p is 13 times longer than that of the fully swollen state [Fig. 7(a)]. As temperature is increased to 293 K and the number of DMF bridges is reduced by half, as shown in Fig. 5(b), l_p is increased but merely by a factor of 4 [Fig. 7(b)]. For the chains with $N_l = 150$, which are collapsed by ten DMF bridges at the maximally collapsed state [Fig. 5(d)], l_p is even increased by about a factor of 180 [Fig. 7(c)]. When $x_c > x_c^*$, the persistence length l_p decreases concurrently with the reduction in the number of DMF bridges. The analysis also shows that when $x_c \to 1$ the persistence length varies between 32 and 45 Å, which are larger than those at $x_c \approx 0$.

The chain stiffness can be evaluated by the ratio of the persistence length to the contour length [54]. The results are shown in Fig. 8(a). In the limit of $l_p/L_C \ll 1$, a chain essentially retains inherent flexibility at a large scale. In the opposite limit of $l_p/L_C \gg 1$, a chain will behave like a rod structure. Figure 8(b) shows that l_p is larger than L_C when the number of the cosolvent bridges n_C^B exceeds about 5, which can be regarded as an onset of chain stiffness driven by the cononsolvency effect. In terms of l_p/L_C, the chain with $N_l = 22$ essentially retains the inherent stiffness at 293 K, but becomes more rigid at 278 K. For $N_l = 150$, l_p/L_C varies between 4 and 10 in the range $0.25 < x_c < 0.35$ at 293 K. In this case, especially for the maximum $l_p/L_C = 10$ with ten DMF bridges, the chains will be zippered by the cosolvent bridges to be a rodlike structure, where the cosolvent bridging polymer extraordinarily suppresses the thermal fluctuations. It is worth noting that the persistence length l_p of constrained chains can be comparable to or longer than length scales on which polymer chains are constituted such as end-to-end distance and contour length, although the flexibility of free PNIPAM chains may not be significantly affected by temperature and cononsolvency [49]. However, for most of the DMF concentrations, the longer chain $N_l = 150$ is much more flexible than the shorter chain $N_l = 22$ in terms of the ratio l_p/L_C [Fig. 8(a)].

The persistence length of individual chains is intently associated with macroscopic properties of polymers [55]. The

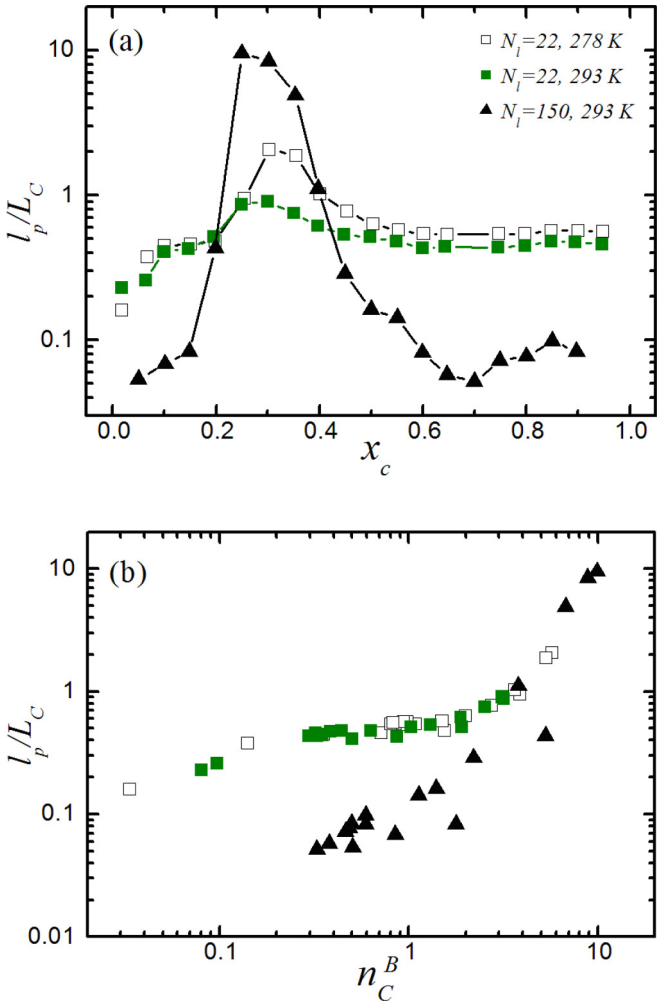

FIG. 8. (a) l_p/L_C as a function of x_c. (b) l_p/L_C as a function of DMF bridge number per chain n_C^B.

cononsolvency-induced chain stiffness of PNIPAM microgels is compared with the temperature-strengthened modulus in pure water. Tagit *et al.* [39] and Hashmi and Dufresne [37] reported that Young's modulus of PNIPAM microgels increases by a factor of 10 when temperature is raised over T_{LCST}. Tagit *et al.* also found that the surface stiffness decreases by about a factor of 100 when the dry microgel is swollen in water below T_{LCST} [39]. Voudouris *et al.* reported that the compressive elastic modulus increases by a factor of 10 with temperature [40]. For interfacial PNIPAM microgels, Schmidt *et al.* found that Young's modulus of microgel films increases by a factor of 7 [41]. Obviously, our results for the cosolvent-induced chain stiffness are in good agreement with these existing experimental data, which provides a predictive understanding of the cononsolvency effect on the suspension mechanical properties of PNIPAM microgels at $T < T_{\mathrm{LCST}}$.

IV. CONCLUSIONS

We have investigated the effect of DMF on the PNIPAM microgel in aqueous solutions. The cononsolvency phenomenon is rationalized by a combination of preferential

adsorption-bridging mechanism and mean-field approaches. All the features of the reentrant transition of PNIPAM microgels are quantitatively correlated to the number DMF bridging adsorptions. Local-bulk partition coefficients for the preferential adsorption of DMF to PNIPAM chains are obtained. The results reveal that the number of DMF bridges per chain, which controls the extent of the cosolvent-included collapse at $T < T_{\mathrm{LCST}}$, decreases with increasing temperature and chain length. In particular, while the DMF bridges incur the conformational shrinking and eventual collapse of the PNIPAM microgel, the nonbridge binding of DMF molecules with PNIPAM microgels continues. Since the molecular affinity of DMF to PNIPAM gets increasingly better with increasing the DMF concentration, the collapse transition of PNIPAM microgels is decoupled from the solvent quality of DMF-water mixtures during cononsolvency.

The cononsolvency effect on the chain flexibility of PNIPAM microgels is analyzed by a mean-field approach that considers the features of PNIPAM microgels including the elasticity of semiflexible chains, the constraint effect of networks and cosolvent bridging, and the surface charge of microgels, in addition to the preferential adsorption-bridging mechanism. The analysis gives rise to a detailed description of the cosolvent-facilitated persistence length of constrained chains at $T < T_{\mathrm{LCST}}$. The results are in good agreement with the existing experimental data regarding suspension mechanical properties of PNIPAM microgels in pure water at $T > T_{\mathrm{LCST}}$.

Our paper provides insights into the cononsolvency phenomenon of thermoresponsive PNIPAM microgels. Pragmatic analysis and verifiable approaches would be useful in the interpretation of cononsolvency effects on constrained polymer systems.

ACKNOWLEDGMENT

We are thankful to the reviewers for bringing [28,29] to our attention.

[1] A. Fernandez-Nieves, H. M. Wyss, J. Mattsson, and D. Weitz, *Microgel Suspensions: Fundamentals and Applications* (Wiley-VCH, Weinheim, 2011).
[2] P. J. Yunker, K. Chen, M. D. Gratale, M. A. Lohr, T. Still, and A. G. Yodh, Rep. Prog. Phys. **77**, 056601 (2014).
[3] F. A. Plamper and W. Richtering, Acc. Chem. Res. **50**, 131 (2017).
[4] Y. Lu and M. Ballauff, Prog. Polym. Sci. **36**, 767 (2011).
[5] R. Pelton, Adv. Colloid Interface Sci. **85**, 1 (2000).
[6] A. Halperin, M. Kroger, and F. M. Winnik, Angew. Chem. Int. Ed. **54**, 15342 (2015).
[7] F. M. Winnik, H. Ringsdorf, and J. Venzmer, Macromolecules **23**, 2415 (1990).
[8] H. G. Schild, M. Muthukumar, and D. A. Tirrell, Macromolecules **24**, 948 (1991).
[9] G. Zhang and C. Wu, J. Am. Chem. Soc. **123**, 1376 (2001).
[10] R. O. R. Costa and R. F. S. Freitas, Polymer **43**, 5879 (2002).
[11] L. B. Sagle, Y. Zhang, V. A. Litosh, X. Chen, Y. Cho, and P. S. Creme, J. Am. Chem. Soc. **131**, 9304 (2009).
[12] C. Scherzinger, A. Schwarz, A. Bardow, K. Leonhard, and W. Richtering, Curr. Opin. Colloid Interface Sci. **19**, 84 (2014).
[13] I. Bischofberger, D. C. E. Calzolari, P. De Los Rios, I. Jelezarov, and V. Trappe, Sci. Rep. **4**, 4377 (2014).
[14] D. Mukherji, M. Wagner, M. D. Watson, S. Winzen, T. E. de Oliveira, C. M. Marques, and K. Kremer, Soft Matter **12**, 7995 (2016).
[15] S. Backes, P. Krause, W. Tabaka, M. U. Witt, D. Mukherji, K. Kremer, and R. von Klitzing, ACS Macro Lett. **6**, 1042 (2017).
[16] Y. Zhang and P. S. Cremer, Annu. Rev. Phys. Chem. **61**, 63 (2010).
[17] F. Tanaka, T. Koga, and F. M. Winnik, Phys. Rev. Lett. **101**, 028302 (2008).
[18] D. Mukherji, C. M. Marques, and K. Kremer, Nat. Commun. **5**, 4882 (2014).
[19] J. Heyda, A. Muzdalo, and J. Dzubiella, Macromolecules **46**, 1231 (2013).
[20] J. Dudowicz, K. F. Freed, and J. F. Douglas, J. Chem. Phys. **143**, 131101 (2015).
[21] J. Mondal, D. Halverson, I. T. S. Li, G. Stirnemann, G. C. Walker, and B. J. Berne, Proc. Natl. Acad. Sci. USA **112**, 9270 (2015).
[22] J.-U. Sommer, Macromolecules **50**, 2219 (2017).
[23] W. K. Kim, A. Moncho-Jorda, R. Roa, M. Kanduc, and J. Dzubiella, Macromolecules **50**, 6227 (2017).
[24] A. K. Tucker and M. J. Stevens, Macromolecules **45**, 6697 (2012).
[25] P. W. Zhu and D. H. Napper, Chem. Phys. Lett. **256**, 51 (1996).
[26] C. G. Lopez and W. Richtering, Soft Matter **13**, 8271 (2017).
[27] J.-J. Lietor-Santos, B. Sierra-Martin, R. Vavrin, Z. Hu, U. Gasser, and A. Fernandez-Nieves, Macromolecules **42**, 6225 (2009).
[28] R. Keidel, A. Ghavami, D. M. Lugo, G. Lotze, O. Virtanen, P. Beumers, J. S. Pedersen, A. Bardow, R. G. Winkler, and W. Richtering, Sci. Adv. **4**, eaao7086 (2018).
[29] S. Maccarrone, C. Scherzinger, O. Holderer, P. Lindner, M. Sharp, W. Richtering, and D. Richter, Macromolecules **47**, 5982 (2014).
[30] C. M. Hansen, *Hansen Solubility Parameters: A User's Handbook* (CRC, Boca Raton, FL, 2007).
[31] J. S. Palmer and M. C. Boyce, Acta Biomater. **4**, 597 (2008).
[32] C. P. Broedersz and F. C. MacKintosh, Rev. Mod. Phys. **86**, 995 (2014).
[33] I. Teraoka, *Polymer Solutions: An Introduction to Physical Properties* (Wiley, New York, 2002).
[34] E. S. Courtenay, M. W. Capp, C. F. Anderson, and M. T. Record, Jr., Biochemistry **39**, 4455 (2000).
[35] D. R. Canchi and A. E. Garcia, Annu. Rev. Phys. Chem. **64**, 273 (2013).
[36] J. Smiatek, J. Phys.: Condens. Matter **29**, 233001 (2017).
[37] S. M. Hashmi and E. R. Dufresne, Soft Matter **5**, 3682 (2009).
[38] B. Sierra-Martin, Y. Laporte, A. B. South, L. A. Lyon, and A. Fernandez-Nieves, Phys. Rev. E **84**, 011406 (2011).
[39] O. Tagit, N. Tomczak, and G. J. Vancso, Small **4**, 119 (2008).

[40] P. Voudouris, D. Florea, P. van der Schoot, and H. M. Wyss, Soft Matter **9**, 7158 (2013).
[41] S. Schmidt, M. Zeiser, T. Hellweg, C. Duschl, A. Fery, and H. Mohwald, Adv. Funct. Mater. **20**, 3235 (2010).
[42] S. Backes, P. Krause, W. Tabaka, M. U. Witt, and R. von Klitzing, Langmuir **33**, 14269 (2017).
[43] P. W. Zhu and L. Chen, Phys. Chem. Chem. Phys. **19**, 31362 (2017).
[44] J. R. Blundell and E. M. Terentjev, Macromolecules **42**, 5388 (2009).
[45] S. F. Edwards and K. F. Freed, J. Phys. A **2**, 145 (1969).
[46] L. Pescosolido, L. Feruglio, R. Farra, S. Fiorentino, I. Colombo, T. Coviello, P. Matricardi, W. E. Hennink, T. Vermonden, and M. Grassi, Soft Matter **8**, 7708 (2012).
[47] J. Zhou, J. Wei, T. Ngai, L. Wang, D. Zhu, and J. Shen, Macromolecules **45**, 6158 (2012).
[48] M. Braibanti, C. Haro-Perez, M. Quesada-Perez, L. F. Rojas-Ochoa, and V. Trappe, Phys. Rev. E **94**, 032601 (2016).
[49] A. C. Kumbharkhane, S. M. Puranik, and S. C. Mehrotra, J. Solution Chem. **22**, 219 (1993).
[50] E. Kutnyanszky, A. Embrechts, M. A. Hempenius, and G. J. Vancso, Chem. Phys. Lett. **535**, 126 (2012).
[51] J. Ricka, H. Gysel, J. Schneider, R. Nyffenegger, and T. Binkert, Macromolecules **20**, 1407 (1987).
[52] T. Binkert, J. Oberreich, M. Meewes, R. Nyffenegger, and J. Ricka, Macromolecules **24**, 5806 (1991).
[53] B. J. Haupt, T. J. Senden, and E. M. Sevick, Langmuir **18**, 2174 (2002).
[54] Z. Ahmed, E. A. Gooding, K. V. Pimenov, L. Wang, and S. A. Asher, J. Phys. Chem. B **113**, 4248 (2009).
[55] M. Rubinstein and R. H. Colby, *Polymer Physics* (Oxford University, New York, 2003).